Magneto-Rheological Damper - An Experimental Study

Jorge De-Jesus Lozoya-Santos, Rubén Morales-Menéndez, Ricardo Ramirez-Mendoza, Juan C. Tudon-Martinez, Olivier Sename, Luc Dugard

MAGNETO-RHEOLOGICAL DAMPER – AN EXPERIMENTAL STUDY

Jorge de-J Lozoya-Santos, Ruben Morales-Menendez, Ricardo Ramirez-Mendoza, Juan C. Tudón-Martínez
PhD student,
School of Engineering
Tecnologico de Monterrey, Campus Monterrey,
Av E. Garza Sada 2501, Col. Tecnológico, Monterrey, Nuevo León
64849, México
Email: {jorge.lozoya, rmm, ricardo.ramirez, jc.tudon.phd.mty}@itesm.mx

Olivier Sename, Luc Dugard
Institute Polytechnique of Grenoble
Rhone Alpes, France F-38402, Email: {olivier.sename,luc.dugard}@gipsa-lab.grenoble-inp.fr

*A Magneto-Rheological (*MR*) damper is evaluated under exhaustive experimental scenarios, generating a complete database. The obtained database includes classical tests and new proposals emphasizing the frequency contents. It also includes the impact of the electric current fluctuations. The variety of the performed experiments allows to study the* MR *damper force dynamics. A brief description of the damper behavior and a categorization of experiments based on driving conditions and target applications on vehicle dynamics is discussed. The identification of two* MR *damper models as well as their cross validation emphasize the importance of the persistence of experimental inputs and the combinations of rod displacement and electric current sequences for better modeling. New findings in Design of Experiments for model identification are presented.*

1 Introduction

A Magneto-Rheological (*MR*) damper is a hydraulic monotube damper whose oil has metallic particles and its damping coefficient varies according to the supplied electric current. This device performs *actuation* in a semi-active automotive control. Semi-active control strategies are used in automotive primary suspensions, (Lam and Liao, 2003; Song and Ahmadian, 2005; Savaresi and Spelta, 2007; Poussot-Vassal et al., 2008; Choi and Sung, 2008), aeronautics, (Wei and Pinqi, 2007), seismic mitigation in structures, (Luo et al., 2001; Xu et al., 2003; Ikhouane et al., 2005; Cho et al., 2005), washing machines, (Spelta et al., 2009), human prosthetics, (Herr and Wilkenfeld, 2003), among others. An *MR* damper has good industrial features, *Lord*[1], as:

1. *Mass production*: Mechanical simplicity given that it is physically the same as a passive damper.
2. *Efficiency*: The device can change the damping coefficient in *40 ms*, (Koo et al., 2006), over high dynamic range of piston displacements (frequency bandwidth). It also offers a high dissipative force independent of velocity.
3. *Energy*: Low power requirements (12 volts @ 3 A)
4. *Performance*: Large force capacity (3 kN), robustness on heavy duty applications as well as consistent efficacy across extreme temperature variations, and inherent system stability (no active forces generated).

The research on *MR* damper modeling have been done using several approaches for more than *20* years. The main approaches are: physical meaning of the parameters, (Spencer Jr et al., 1997), hysteresis based, (Guo et al., 2006), blackbox models,(Choi et al., 2001; Savaresi et al., 2005), damping and stiffness coefficients as main damping force contributors, (Choi et al., 1998), among others. The common drawback of the later models is that they are not adequate for controller synthesis.

Approaches in control strategies can be classified as: (a) linear controllers using linearized *MR* damper models, mixed sky-hook, (Savaresi and Spelta, 2007), H_2 + Linear-Gaussian-Quadratic (LGQ), (Cho et al., 2005), H_∞, (Du et al., 2005; Choi and Sung, 2008), (b) nonlinear control techniques such as Lyapunov techniques, (Luo et al., 2001), sliding mode control, (Lam and Liao, 2003), Linear Parameter Varying / H_∞, (Poussot-Vassal et al., 2008), adaptive, (Spelta et al., 2009), and (c) intelligent control approaches as Artificial Neural Networks based, (Wang and Liao, 2001; Xu et al., 2003; Lozoya-Santos et al., 2009d; Wei and Pinqi, 2007) and heuristic rules, (Herr and Wilkenfeld, 2003).

A Design of Experiments (*DoE*) that exhaustively explore the behavior of an automotive *MR* damper is proposed.

[1] http://www.lord.com

Table 1. Nomenclature

Var	Description
c_{MR}	Proportional rate of damping in post-yield region
c_p	Viscous damping coefficient, without electric current
$\|\|e\|\|$	Error norm
f_c	Frequency of the piston displacement
f_{cq}	The q^{th} value of the frequency of the piston displacement within a set of Q frequency values
f_I	Damping force due to electric current
f_{MR}	*MR* damping force.
f_p	Passive force due to the mechanical properties
$\hat{f}_{type}$	Estimation of a type of force
g(·)	Nonlinear function
h_x	Hysteresis coefficient due to piston displacement
$h_{\dot{x}}$	Hysteresis coefficient due to piston velocity
i	i^{th} sample of experimental signal
k	Receding horizon for computing $\|\|\|\dot{x}\|\|\|_\infty$
k_{MR}	Stiffness coefficient depending on the electric current
k_p	Stiffness coefficient without electric current
u_c	Controller output for a semiactive suspension
x	Displacement on the *MR* damper piston
$\dot{x}$	Displacement velocity on the *MR* damper piston
x_{peak}	Peak displacement
x_{pp}	Peak to peak displacement
$y_{MR}(I)$	Description of electric current function
I	Electric current
I_q	The level change of the electric current
$PTIC(\cdot)$	Pattern Training Input where $(\cdot)$ can be I or x
β, ρ	Nonlinear function used to estimate variable force dissipation
ζ_I	Damping ratio depending on the applied current
$\tau_{\|I\|}$	Duration in seconds of the applied current value
τ_{MR}	Time constant, 1^{st} order transfer function $f_{MR}(s)/I(s)$
$\frac{Cycles}{\Delta(variable)}$	Periods per change of a variable
$\frac{\Delta(I)}{PTIC(I)}$	Electric current changes per electric current sequence
$\Delta(signal)$	Discrete changes of a signal per complete experiment
$\frac{d(I)}{dt}$	Slope of electrical current
τ_{vco}	Duration of the frequency value in the modulation
ε	Constant for bounding the maximum damping coefficient
$\|\|\|\dot{x}\|\|\|_\infty$	The infinite norm of the absolute deflection velocity $\dot{x}$

The objectives are: to observe the *MR* damper under operating conditions, and to state the ideal *DoE* that identify the damper characteristics. These characteristics are: the transient response of the *MR* force due to an electric current change, the *MR* damping force relation with the displacement, velocity and acceleration of the damper rod, the hysteresis, and the effect of the manipulation shape on the damper case temperature and damping force.

The experimental setup consists of a particular Commercially available Off-The-Shelf *ACDelco*^{TM} *MR* damper which is used for the suspension of a 2008 Cadillac^{TM} vehicle. Even this, the methodology may be extended to any kind of shock absorbers. The identification of an *MR* damper model shows the added-value of the database.

This paper is structured as follows. The main concepts for *MR* damper modeling are presented in section 2. Section 3 reviews the experimental research work, and presents the experimental system as well as the *DoE*. The discussion of findings are presented in section 4. Section 5 presents a study case. Finally, section 6 concludes the research. Table 1 describes the nomenclature.

2 *MR* Damper Modeling

The mechanical damping force of a damper must be described using the rod displacement x and piston velocity $\dot{x}$, (Fukushima et al., 1983). In an *MR* damper, the electric current I varies the oil viscosity, changing the generated mechanical damping force, (Kordonsky, 1993). The operating range of an *MR* damper for comfort and road holding conditions is shown in their force-velocity *(F-V)* characteristic under a fluctuating electric current. The *F-V* characteristic have yield points that consist of damping force and a given piston velocity. The yield points vary due to mechanical and electric current magnitudes changes and exhibits hysteresis.

MR damper modeling approaches can be classified as either static or dynamic. A *static MR* damper model estimates the generated force using the instantaneous electric current and displacement/velocity and not earlier values. In a *dynamic MR* damper modeling approach, each model variable can vary without direct exogenous influence. A typical classification of *MR* damper modeling has been based in all the known model approaches: phenomenological (parameters whose meaning is related to the mechanical parts, physical meaning), semi-phenomenological (parameters with physical meaning) and black-box (parameters without physical meaning). A new classification for modeling is proposed based on its original structure as: passive or I-driven.

A passive model is valid under the assumption that the damper is filled with an *MR* fluid, and its objective is to successfully model the hysteretic and nonlinear behavior of the device under constant electric current. Therefore, it does not include the electric current as an input variable. Representative passive models are: Bingham, (Stanway et al., 1987), Bouc-Wen Modified, (Spencer Jr et al., 1997), Polynomial, (Choi et al., 2001), Semi-Phenomenological, (Guo et al., 2006), Phase-Transition, (Wang and Kamath, 2006), and Three-parameters, (Choi and Sung, 2008). These models study the force-velocity and transient response curves.

An I-driven model includes the electric current as input variable and its formulation is based on two assumptions: the damper includes an *MR* fluid as oil and the persistent fluctuation of electric current. Ideally, this model structure

(1-1) of a damper with an *MR* fluid can be represented as equivalent to two dampers in parallel: a damper with constant shear stress (passive) and a damper with variable-shear stress (semi-active) due to the variation of the applied electric current. The sum of the two components yields the total *MR* damping force f_{MR}.

$$f_{MR} = f_p(x,\dot{x}) + f_I(x,\dot{x},I) \quad (1\text{-}1)$$
$$f_p = k_p x + c_p \dot{x} \quad (1\text{-}2)$$
$$f_I = y_{MR}(I) \cdot g(\dot{x},x) \quad (1\text{-}3)$$

where $g(\dot{x},x)$ is a nonlinear function. It is not surprising that black-box approaches obtain the best results: Nonlinear Auto Regressive with eXogenous (*NARX*) input model, (Lozoya-Santos et al., 2009b), and *NARX* based on Neural Networks (*NNARX*) (Burton et al., 1996; Wang and Liao, 2001, 2005; Savaresi et al., 2005; Boada et al., 2008; Lozoya-Santos et al., 2009c). The state of the art model approaches are: (a) the modified Bouc Wen with polynomial dependence on electric current, (Spencer Jr et al., 1997), and (b) the black-box approaches.

For designing an automotive suspension control system, an *MR* damper model can range from a complex one (high performance simulation) to a simple one (for controller synthesis). For controller synthesis, the model features are: (a) it must be I-driven, (b) comfort and road holding domains must be met, (c) experimental dataset must consider persistent inputs that represent the typical operating conditions.

2.1 A Modified Semi-Phenomenological Model

A modified version of the semi-phenomenological model (Guo et al., 2006) where the force of the damper is described by: (a) the force due to the spring effect of the gas accumulator, (b) the damping force due to the oil viscosity, and (c) the *MR* force due to the electric current, (Lozoya-Santos et al., 2009a). This approach assumes a non significative effect of the electric current on damping coefficient for low velocities. In a tradeoff velocity value the magnetic links in the *MR* fluid are broken by the stress changing the damping coefficient. This coefficient remains the same until the links are joined, a phenomenon depending on the velocity, (Jolly et al., 1998). When the magnetic links are rejoined, the magnetic hysteresis mixed with a increasing velocity in inverse direction generates hysteresis in the *F-V* characteristic. The observed consequence is a proportional effect of the electric current on the maximum f_{MR}:

$$f_{MR} = u_c \cdot c_{MR} \cdot \beta + c_p \dot{x} + k_p x \quad (2\text{-}1)$$
$$\beta = tanh(h_{\dot{x}} \dot{x} + h_x x) \quad (2\text{-}2)$$

where u_c is the controller output of a semi-active suspension, c_{MR} is a proportional rate of damping force per ampere over the tradeoff velocity of piston, c_p is a linear viscous damping coefficient, k_p is a linear stiffness coefficient, $h_{\dot{x}}$ is a hysteresis coefficient due to the velocity of piston, h_x, is a hysteresis coefficient due to the displacement of piston, β describes the damping force behavior due to the friction and activation of the symmetrical blow-off valves.

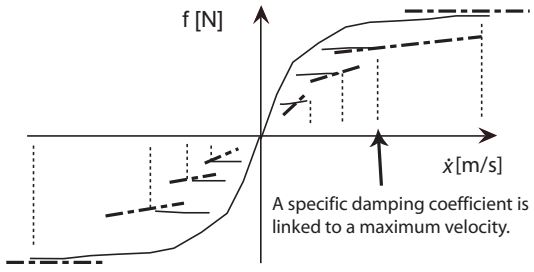

Fig. 1. The damping coefficient versus maximum deflection velocity.

2.2 The Maximum Deflection Velocity (VMax) model

The model is based on the variation of the *postyield* damping coefficient depending on the maximum deflection velocity, (Lozoya-Santos et al., 2010). The maximum deflection velocity is a function of the maximum amplitude and the frequency of the deflection, (Bastow et al., 2004). Hence this measure can capture the dynamic behavior of the damping coefficient, such as,

$$\zeta_I = \frac{f_I}{\dot{x}} = \frac{y_{MR}(I) \cdot g(\dot{x},x)}{\dot{x}} \propto \frac{I \cdot c_{MR}}{|||\dot{x}|||^{i}_{\infty_{i-k}}} \quad (3\text{-}1)$$
$$f_I \longmapsto \zeta_I \cdot \dot{x} \propto \frac{I \cdot \dot{x} \cdot c_{MR}}{|||\dot{x}|||^{i}_{\infty_{i-k}}} \quad (3\text{-}2)$$

where ζ_I is the damping ratio depending on the electric current, f_I is the damping force due to the change of oil viscosity caused by the electric current fluctuation, i is the instantaneous sample of the measured $\dot{x}$, k is an integer subscript meaning the receding horizon to compute the maximum absolute velocity represented by $|||\dot{x}|||^{i}_{\infty_{i-k}}$, i. e. the infinite norm of the velocity of the piston, $\dot{x}$. Figure 1 shows how the damping coefficient changes with maximum velocity, where the dashed lines are the damping coefficient trajectories that depend on the interval of $\dot{x}$. The model is:

$$f_{MR} = u_c \cdot c_{MR} \cdot \rho + c_p \dot{x} + k_p x \quad (4\text{-}1)$$
$$\rho = \dot{x} \cdot \frac{1}{|||\dot{x}|||^{i}_{\infty_{i-k}} + \varepsilon} \quad (4\text{-}2)$$

where ρ describes the damping force behavior due to the friction and the activation of the symmetrical blow-off valves.

3 Design of Experiments (*DoE*) for *MR* damper models

The *DoE* for the *MR* damper consists of a pair of training sequences: displacement and electric current. Table 2 summarizes various works from the point of view of experimentation. Important findings can be summarized as follows:

1. The *DoE* for identification of *MR* damper models have not precisely been focused on a specific application.

2. Commonly, the bandwidth of the damping manipulation signal has not been addressed.
3. The effect of inputs on the temperature and force of the *MR* damper has not usually been fully explored.
4. The *DoE* ordinarily exhibit a lack of high-frequency bandwidth in the piston displacements.
5. The persistent exploration of the force-velocity diagram mostly has not been an objective.
6. The number of experiments usually is high and only static information is retrieved, (9 in (Burton et al., 1996), 392 in (Nino et al., 2008)).
7. The experiments commonly have long duration.
8. The good models for the *F-V* diagram mostly were identified with low displacement frequencies.
9. The number of experiments usually is less than 5 for persistent displacement signals.

The best practices could be:

1. It is possible a better identification of *MR* damper model parameters with the data obtained from random displacement sequences rather than harmonic displacements, (Burton et al., 1996).
2. For a displacement bandwidth below *2* Hz, the force is strongly dependent on the frequency. Over *4* Hz, the nonlinear force appears due to the inertial effect of the *MR* fluid, (Li et al., 2000).
3. There is a nonlinear induced effect on the *MR* force caused by the velocity, (Bastow et al., 2004).
4. The amplitude of the displacement is not significant in the magnitude of the f_{MR}, meanwhile the frequency of the displacement has a high nonlinear effect. The electric current has the strongest effect, (Shivaram and Gangadharan, 2007).

Taking into account that the *MR* damper has a typical damper mechanical structure, some important observations on damper testing, (Kowalski et al., 2001), are extrapolated to the *MR* damper experimentation in order to define the *DoE*:

1. The temperature of the damper must be monitored throughout the experiment.
2. The stroke must be the same between experiments if the resultant identified models are going to be compared.
3. The sine-on-sine displacements identify frequency dependent parameters, hence the models tend not to be generalized.
4. The sine-on-sine displacements and the harmonic displacement show different parameters when the identification is applied to the same model.
5. The parameters derived from random and swept sinusoidal displacements converge to similar values and good models in restricted bandwidths.
6. The *DoE* with sequences of electric current in a bandwidth $0-10$ Hz and piston displacement in a bandwidth $0-15$ Hz need less experimentation time
7. A model without parameters skew can be found using one test.

Based on the literature review, twelve training sequences are presented (some are new proposals). The training sequences focus on the shape of the *MR* damper piston displacement and the electric current through the *MR* damper coil.

The objectives of the *DoE* are: (a) define the interactions between the velocity, displacement, and electric current, (b) analyze the impact of the *DoE* in the identification process, (c) find the best training sequence for *MR* dampers modeling, and (d) design and identify models for controller synthesis, and (e) identify models for specific driving and target applications.

3.1 Displacement Sequences.

The common displacement features for the proposed sequences are (a) a bandwidth between *0.5* and *14.5* Hz, and (b) a maximal displacement of *7.6* mm for symmetric signals and *12.7* mm for random signals, Fig. 2.

1. Road Profile *Smooth highway* (*RP*). *RP*s have been utilized as a test signal for passive damper experiments, (Kowalski et al., 2001), and in the training of *MR* damper artificial neural network models, (Savaresi et al., 2005). The objective is to test the *MR* damper under standard automotive conditions. The displacements were based on the specification of the spectral density of several road profiles, (Wong, 2001). These are computed using an algorithm based on the Fourier inverse transform, (da Silva, 2004). The *RP smooth highway* is the most common for commercial vehicles.
2. Sinusoidal signal with stepped Frequency and constant amplitude Signal (*SFS*). The *SFS* is an usual displacement sequence in the *DoE* for *MR* dampers, (Burton et al., 1996), (Spencer Jr et al., 1997), (Li et al., 2000), (Kowalski et al., 2001), (Xia, 2003), (Wang and Kamath, 2006), (Guo et al., 2006), (Nino et al., 2006), and (Shivaram and Gangadharan, 2007). The sinusoidal displacement has a constant frequency and a constant amplitude. Hence, the experimentation with a *SFS* sequence could derive in long duration experiments and a redundant dynamics exploration. The frequency of the signal is increased *0.5* Hz each *3* or *6* displacement periods. It is important to include the transient response due to abrupt frequency changes. This in order to capture a rich exploration of the specimen in short time.
3. Sinusoidal CHirp Signal (*CHS*). The *CHS* is a sinusoidal signal with a constant amplitude and linear frequency increments through the experiment.
4. Frequency Modulated - (*FM*). The frequency is varied uniformly in the bandwidth with a constant amplitude. This pattern is created using a voltage controlled oscillator. The supplied voltage is a stepped signal whose steps have finite duration, named Increased Clock Period Signal (*ICPS*), (Söderström and Stoica, 1989). The step duration is *200* ms. This duration guarantees full cycles of displacement over *5* Hz. The signal frequency output is proportional to the supplied voltage.
5. Triangular wave with Positive and Negative Variable Slopes Signal (*TPNVS*). This signal consists of a posi-

Table 2. Comparison of training inputs. First column is the model name, second column specifies inputs. Columns F-V and F-D are for Force-Velocity and Force-Displacement diagrams of predicted force versus experimental force. Cost function is the index fitting performance; d [mm] refers to amplitude in displacement; Hz is the frequency bandwidth and eXogenous input being current or voltage. Each one could have two values, first is the maximum tested value and second is the number of tested values. Other case is if there is only one maximum value reached for the respective signal. Finally, two values separated by a dash means the span of continuous variations.

Model	Training	F-V	F-D	Cost function	d[mm]	Hz	eXogenous
Bingham and Bouc Wen (1997)	Sinusoidal displacement with increasing	yes	yes	$\|e\|$	25	4,4	1A,4
3 parameters (1998; 2008)	frequency and constant current	yes	yes	$\|e\|$	25	2,3	2A,6
Phase transition (2006)		yes	no	Sum of Square Errors (*SSE*)	25	4,5	1A,4
Statistical (2007)		no	no	Root Mean Square (*RMS*)	3,1	8,2	60 and 120A-t
Statistical (2007)		no	yes	RMS	3	8,3	40, 80 and 120A-t
Semi-physical (2006)		yes	yes	SSE	20,3	4,5	2A, 5
NARX (2006)		yes	yes	*ESR*	40,3	14.5,28	4A,14
ANNARX (1996)	Band-limited white	no	yes	RMS	10	1.5,1	$3\frac{kV}{mm}$,2
	noise as displacement	no	yes	RMS	5	4,1	$3\frac{kV}{mm}$,2
	and constant current	no	yes	RMS	5	4,1	$3\frac{kV}{mm}$,2
ANNARX (2005)		no	no	SSE	25	3,2	12V,3
ANNARX (2005)		no	no	ESR	25	15	1.2A,3
Phase transition (2006)	Sinusoidal displacement and constant current	yes	no	SSE	25	2.5	0.5A
Blind Hammerstein (2007)	ICPS (1989) and constant current	no	no	$\|e\|$	0-15	0-5	1.25V
ANNARX (2002)	Band-limited white	no	no	SSE	22	1-5	0-3V
	noise as displacement	no	no	SSE	0-1	3-6	0-2.25V
ANNARX (2005)	and current	no	no	SSE	0-25	0-3	0-6V
ANNARX (2005)		yes	yes	SSE	0-20	1-5	0-2.25V
ANNARX (2003)	Sinusoidal displacement and ramp current	no	no	$\|e\|$	15	2.5	0-2.25V
ANNARX (2005)	Band white noise limited displacement and stepped current	no	no	SSE	25	3,2	12V
ANNARX (2005)	Band white noise limited displacement and APRBS (1989)	no	no	ESR	0-25	0-15	0-1.2A

tively sloped ramp followed by a negatively sloped one. From origin (*0* mm), the ramp with positive slope raises to *7.6* mm, then it continues with a negative slope until reaching *-7.6* mm. It changes again to positive slope and returns to origin. The slope is increased every 3 or 6 periods, depending on the experiment. The slope increment stops when the *TPNVS* period is equal to *1/14.5* Hz.

6. Amplitude Modulated Signal (*AM*). The *AM* is a modification of the well know signal in communications engineering. The amplitude changes with a stepped shape each 3 cycles of the carrier frequency. Each sequence has *200* uniformly distributed amplitude levels. The objective is to obtain the f_{MR} on a fixed carrier frequency and random stepped amplitudes. This sequence is oriented to the identification of Linear Parameter-Varying *MR* damper models, where the scheduling variable is the oscillation frequency.

3.2 Electric Current Sequences.

The electric current span is between 0 to 2.5 A for the proposed sequences. Six sequences for this input are described in Figure 3.

1. Stepped electric Current increments (*SC*). The utilization of a constant electric current in the experimenta-

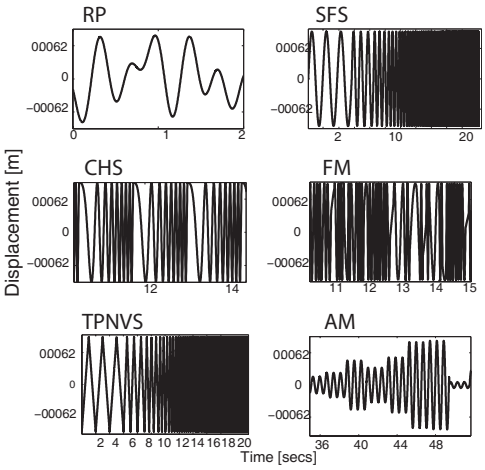

Fig. 2. Training displacement sequences for model identification.

tion over *MR* dampers allows for the observation of the f_{MR} operation zones. A stepped increment of the electric current value covering the full span is proposed. The stepped increment will depend on the experiment. The duration of the step is defined by the duration of the displacement pattern.

2. Positive variable slope Ramp (*RC*). The *RC* begins from zero and finishes in the maximum electric current, then it starts over, (Chang and Zhou, 2002). The coil excitation with several slopes allows for the exploration of the effect of the ratio A/secs over the *MR* force.
3. Ramp with Positive and Negative Variable Slopes (*RPNVS*). The *RPNVS* begins from zero raising to the maximum electric current with a specified positive slope. The signal continues with the same slope but with a negative sign until reaching *0* A. The *MR* fluid has a hysteretic behavior on the magnetization of the metallic particles. The combination of this magnetization with the accumulator effect over the *MR* damper could be emphasized using this sequence.
4. Increased Clock Period Signal (*ICPS*). This signal is the same used in the *FM* signal generation. In this case, the step duration must be at least equal to the settling time of the f_{MR}, $4 \cdot \tau_{MR}$ ms. τ_{MR} is the time constant of the first order transfer function $f_{MR}(s)/I(s)$, (Koo et al., 2006). The damping change reaches is steady state at $4 \cdot \tau_{MR}$ ms. The objective is to extract the steady and transient behavior of the f_{MR} due to the persistence magnetic excitation of the *MR* fluid.
5. Amplitude Pseudo Random Binary Signal (*APRBS*). This is a stepped signal where the amplitude and the step duration change randomly, (Söderström and Stoica, 1989). This electric current sequence has been used in order to fit an Artificial Neural Network model of an *MR* damper, (Savaresi et al., 2005). When the *MR* damper is subjected to an *APRBS* electric current, the f_{MR} could not get to a steady state due to the magnetic links of the metallic particles not being fully aligned. This is true only if the minimum *APRBS* step duration is not, at least, equal to the settling time of the f_{MR}.
6. Pseudorandom Binary Signal (*PRBS*). This test is usually exploited for process identification in domains such as *MR* dampers. The common units are voltage but in this work they are proposed as amperes because these are the more realistic manipulation units in a semi-active control strategy.

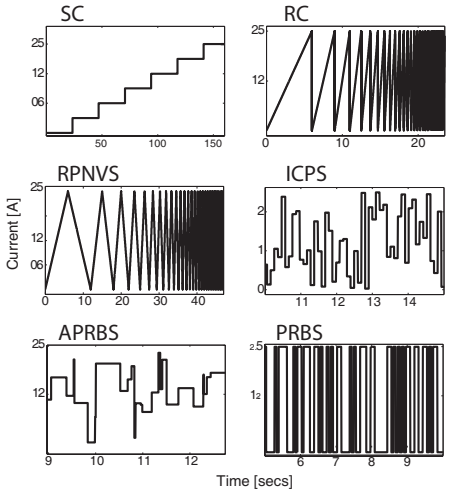

Fig. 3. Training electric current sequences for model identification.

Several *DoE* were proposed, Table 3. Each proposed experiment has the following scope:

a. To perform an analysis of the effect of the input variables on the f_{MR} by employing the surface response method and to define their level of significance for the estimation of the output. The analysis includes the linear, quadratic, and crossed interaction of the inputs, (Experiment # 1).

b. To analyze f_{MR} response when submitted to step changes of the electric current and define the bandwidth of this transfer function, (Experiment # 2).

c. To observe the *MR* damper behavior under constant electric currents in the frequency bandwidth of displacement for automotive applications, (Experiments # 3 and # 21-29).

d. To explore the f_{MR} gain with regard to a constant ratio change in the applied electric current when a harmonic displacement is applied, (Experiment #4). Emphasis is made on the magnetic hysteresis effect in the *MR* fluid, (Experiment # 5).

e. The exhaustive exploration of the f_{MR} in low displacement velocities, in order, to determine if this dynamic information identifies generalized models for several types of excitation (Experiment #6 with *ICPS* and Experiment # 7 with *PRBS*).

f. To compare the f_{MR} obtained from a repetitive electric current sequence in order to validate the independence of the damping variation from the frequency of the displacement for several types of excitation (Experiment # 8 with *ICPS* and Experiment # 9 with *PRBS*).

Table 3. Design of Experiments. First column enumerates the DoE. The second and third columns define the sequences for displacement and electric current. The fourth and fifth columns specify the characteristics of each sequence. Time specifies the experiment duration. Table 1 describes the nomenclature.

n	x	I	Displacement [mm] $\frac{Cycles}{\Delta(f_c)}$	$Time$ [s]	Electric Current [A]	$\frac{PTIC(I)}{PTIC(d)}$
1	AM	SC	$\frac{Cycles}{\Delta(f_c)}$=4, see Table 5	16	$\frac{\Delta(I)}{PTIC(I)} = 1$, see Table 5	1
2	TPNVS	SC	$\frac{d(x)}{dt} = \frac{32}{f_{ci}} \frac{mm}{t}$, $\frac{Cycles}{\Delta(f_c)}$=3, $f_c = \{0.5, 1, \ldots, 14.5\}$, $x_{pp} = 16mm$	24	$\frac{\Delta(I)}{PTIC(I)} = 3$, $I = \{0.5, 2\}A$	$\frac{3}{f_{ci}}$
3	SFS	SC	$\frac{Cycles}{\Delta(f_c)}$=3, $f_c = \{0.5, 1, \ldots, 14.5\}$, $x_{pp} = 16mm$	237	$\frac{\Delta(I)}{PTIC(I)} = 8$, $I = \{0, 0.4, \ldots, 2.4\}A$	$\frac{\Delta(I)}{28\Delta(f_c)}$
4	SFS	RC	$\frac{Cycles}{\Delta(f_c)}$=3, $f_c = \{0.5, 1, \ldots, 14.5\}$, $x_{pp} = 16mm$	24	$\frac{d(I)}{dt} = \frac{2.5}{f_{ci}} \frac{A}{t}$	$\frac{1}{f_{ci}}$
5	SFS	RPNVS	$\frac{Cycles}{\Delta(f_c)}$=6, $f_c = \{0.5, 1, \ldots, 14.5\}$, $x_{pp} = 16mm$	47	$\lvert \pm \frac{d(I)}{dt} \rvert = \frac{2.5}{f_{ci}} \frac{A}{t}$	$\frac{1}{f_{ci}}$
6	CHS	ICPS	$f_c \in \{0.5, 6\}$, $x_{pp} = 16mm$	30	$\tau_{\lVert I \rVert} = 0.07s$	$\frac{1}{28}$
7	CHS	PRBS	$f_c \in \{0.5, 6\}$, $x_{pp} = 16mm$	30	$\tau_{\lVert I \rVert} \in \{0.05, 0.5\}s$	$\frac{1}{28}$
8	SFS	ICPS	$\frac{Cycles}{\Delta(f_c)} = \frac{2}{f_{ci}}$, $f_c = \{0.5, 1, \ldots, 14.5\}$, $x_{pp} = 16mm$	58	$\tau_{\lVert I \rVert} = 0.100s$	$\frac{1}{f_{ci}}$
9	SFS	PRBS	$\frac{Cycles}{\Delta(f_c)} = \frac{2}{f_{ci}}$, $f_c = \{0.5, 1, \ldots, 14.5\}$, $x_{pp} = 16mm$	58	$\tau_{\lVert I \rVert} \in \{0.05, 0.5\}s$	$\frac{1}{f_{ci}}$
10	FM	ICPS	$\tau(vco) = 0.10s$, $f_c = \{0.5, 14.5\}$, $x_{pp} = 16mm$	30	$\tau_{\lVert I \rVert} = 0.10s$	1
11	FM	PRBS	$\tau(vco) = 0.10s$, $f_c = \{0.5, 14.5\}$, $x_{pp} = 16mm$	30	$\tau_{\lVert I \rVert} \in \{0.05, 0.5\}s$	1
12	RP	ICPS	Smooth highway, $x_{pp} = 25mm$	30	$\tau_{\lVert I \rVert} = 0.100s$	1
13	RP	APRBS	Smooth highway, $x_{pp} = 25mm$	30	$\tau_{\lVert I \rVert} \in \{0.001, 0.5\}s$	1
14	RP	PRBS	Smooth highway, $x_{pp} = 25mm$	30	$\tau_{\lVert I \rVert} \in \{0.05, 0.5\}s$	1
15	RP	APRBS	Smooth highway, $x_{pp} = 25mm$	600	$\tau_{\lVert I \rVert} \in \{0.001, 0.5\}s$	1
16	RP	ICPS	Smooth highway, $x_{pp} = 25mm$	600	$\tau_{\lVert I \rVert} = 0.100s$	1
17	TPNVS	C	$\frac{d(x)}{dt} = \frac{7.62}{f_{ci}} \frac{mm}{t}$, $\frac{Cycles}{\Delta(f_c)}$=3, $f_c = \{0.5, 1, \ldots, 14.5\}$, $x_{pp} = 3.81mm$	96	0, 0.4,0.8,1.2, 1.6, 2.1, 2.5	$\frac{1}{4}$
18	FM	C	$\tau(vco) = 0.10s$,$f_c = \{0.5, 14.5\}$, $x_{pp} = 3.81mm$	120	0, 0.4,0.8,1.2, 1.6, 2.1, 2.5	$\frac{1}{4}$
19	FM	ICPS	$\tau(vco) = 0.10s$, $f_c = \{0.5, 14.5\}$, $x_{pp} = 3.81mm$	120	$\tau_{\lVert I \rVert} = 0.100s$	$\frac{1}{4}$
20	RP	ICPS	Smooth highway, $x_{pp} = 3.81mm$	120	$\tau_{\lVert I \rVert} = 0.100s$	$\frac{1}{4}$
21	AM	ICPS	$\frac{Cycles}{\Delta(x_{peak})}$=3, $f_c = \{1.4, \ldots, 14\}Hz$, $x_{peak} \in \{0.01, 12.5\}mm$	See Table 4	$\tau_{\lVert I \rVert} = 0.10s$	1
22	SFS	C	$\frac{Cycles}{\Delta(f_c)}$=3, $x_{pp} = 25mm$	23	0, 0.4,0.8,1.2, 1.6, 2.1, 2.5	1
23	SFS	C	$\frac{Cycles}{\Delta(f_c)}$=3, $x_{pp} = 16mm$	23	0, 0.4,0.8,1.2, 1.6, 2.1, 2.5	1
24	AM	C	$\frac{Cycles}{\Delta(x_{peak})}$=3, $f_c = \{1.4, \ldots, 14\}Hz$, $x_{peak} \in \{0.01, 12.5\}mm$	46	0, 0.4,0.8,1.2, 1.6, 2.1, 2.5	1
25	TPNVS	C	$\frac{d(x)}{dt} = \frac{32}{f_{ci}} \frac{mm}{t}$, $\frac{Cycles}{\Delta(f_c)}$=3, $f_c = \{0.5, 1, \ldots, 14.5\}$, $x_{pp} = 16mm$	24	0, 0.4,0.8,1.2, 1.6, 2.1, 2.5	1
26	FM	C	$\tau(vco) = 0.10s$, $f_c = \{0.5, 14.5\}$, $x_{pp} = 16mm$	30	0, 0.4,0.8,1.2, 1.6, 2.1, 2.5	1
27	RP	C	Smooth highway, $x_{pp} = 25mm$	30	0, 0.4,0.8,1.2, 1.6, 2.1, 2.5	1
28	RP	C	Smooth highway, $x_{pp} = 25mm$	30	0, 0.4,0.8,1.2, 1.6, 2.1, 2.5	1
29	RP	C	Smooth highway, $x_{pp} = 25mm$	30	0, 0.4,0.8,1.2, 1.6, 2.1, 2.5	1

g. To validate the importance of the frequency randomness in the rod displacement on the f_{MR} when the amplitude is constant for several types of excitation (Experiment # 10 with *ICPS* and Experiment # 11 with *PRBS*).

h. To validate the model identification quality given a realistic displacement and several types of electric current (Experiments # 12, # 13 and #14), when this quality is compared with harmonic-displacement model identifi-

cation (for example, Experiments # 8-11).

i. To observe the effects on the temperature of the f_{MR} when the device is submitted to realistic displacements and several excitation changes over long periods of time, (Experiments # 15 and # 16).

j. To define the influence of the piston position as a factor in the delivered f_{MR} due to the effect of the internal accumulator, when submitted to several types of displacements and excitations, (Experiments # 17-20).

k. To emphasize the effect of the amplitude displacement of rod and the electric current randomness when the frequency of the piston displacement is constant (Experiment # 21) and compared with rich frequency displacements and constant amplitude (Experiments # 1-11).

l. To have a database with the classical experimentation for *MR* dampers (Experiments # 21-29) and to do a comparison with those obtained with a persistent electric current.

3.3 Experimental System

The experimental system consists of three sections: acquisition system, actuation system, and control system. The acquisition system captures three signals: (a) the displacement, (b) the generated force, and (c) the electric current through the *MR* damper coil. The operation of the systems is done via a *Supervisory Control* System *(SCS)*, which is based on *National Instruments* ^{TM} equipment and *LabView*^{TM}. The actuation system is an *MTS*^{TM} equipment that includes: an actuator of *25* kN with a 15 Hz bandwidth, a controller hardware unit *Flextest GT*, a software *Station Manager*^{TM}, and a *MultiPurpose TestWare*^{TM}, see Fig. 4. The load capacity is *25* kN at *20,690* kPa. The stroke is *150* mm. The span of the piston deflection is $\pm$12.5 mm. An electric current driver adjusts the command from *0* to *2.5* A.

4 Experimental results

Various important results were found. These results show the potential application of this research. The factors are: (a) the displacement variation, (b) the effect of the electric current and the frequency of the displacement on hysteresis, (c) the linearity of the generated force with the electric current, and (d) the temperature of the damper. Said phenomena were observed in Experiment # *21* (persistent inputs), Experiment # *22* (classical *DoE*), and Experiment # 26 (persistent frequency of the piston displacement with constant current).

The velocity of damper rod is computed with central differentiation algorithm. Both, rod displacement and velocity are filtered with a Butterworth filter with cut-off frequency of 16 Hz. Figure 5a shows the phase plane obtained after the proposed procedure for Experiment # 21. For displacements in Experiments # 22-29, the central differentiation is enough for the computation.

In the displacement sequence, the amplitude variation is a stronger factor than the frequency is. The vertical uniformity of the covering is caused by the amplitude variation and the applied electric current. The maximum achieved velocity or horizontal covering is a consequence of the carrier frequency, Fig. 5b.

Table 4. Experiment 21_i. Carrier frequencies and the duration.

Subscript i	f_c	secs	Subscript i	f_c	secs
1	1.40	143.36	6	8.38	24.22
2	2.80	71.87	7	9.78	20.70
3	4.19	48.05	8	11.18	17.97
4	5.59	35.94	9	12.57	16.01
5	6.99	28.09	10	13.97	14.45

Table 5. The DoE for Experiment #1 is a central composite design. The factors are: the electric current through MR damper coil, the frequency of the piston displacement and the amplitude of displacement.

Input levels combination	Current(=)A	f_c(=)Hz	x_{peak}(=)mm
1	0.5100	3.8985	1.9500
2	0.5100	3.8985	7.4400
3	0.5100	12.2040	1.9500
4	0.5100	12.2040	7.4400
5	2.0000	3.8985	1.9500
6	2.0000	3.8985	7.4400
7	2.0000	12.2040	1.9500
8	2.0000	12.2040	7.4400
9	0.0000	8.0513	4.7000
10	2.5000	8.0513	4.7000
11	1.2550	1.0662	4.7000
12	1.2550	15.0362	4.7000
13	1.2550	8.0513	0.6200
14	1.2550	8.0513	12.5141
15	1.2550	8.0513	4.7000
16	1.2550	8.0513	4.7000

The maximum *MR* damping force is quasi linear with the applied electric current. Experiment # 21 and # 26 show that when the electric current is increased, the maximum force is also increased in a quasi linear way. Fig. 6a shows how the larger the electric current, the greater the maximum F_{MR} is. The variations between maximum and minimum forces are consequence of the displacement. Fig. 6b shows the proportional increment on the maximum force when the electric current is increased.

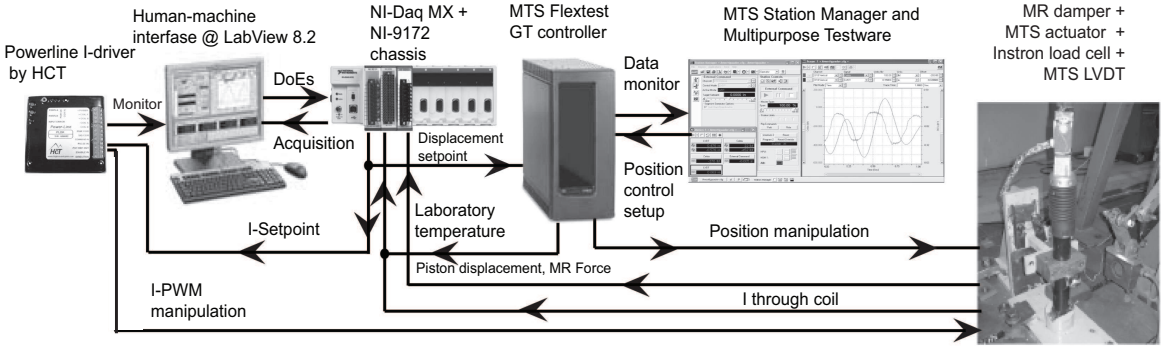

Fig. 4. Experimental system. The lines with arrows show the signals interaction between the experimental setup components. DoE: design of experiment; MR: magnetorheological; HCT: High Country Tek Inc; LVDT: Linear Variable Differential Transformer; ANNARX: Artificial Neural Networks and Auto Regressive with eXogenous input; I-PWM: Electric Current via Pulse Width Modulation.

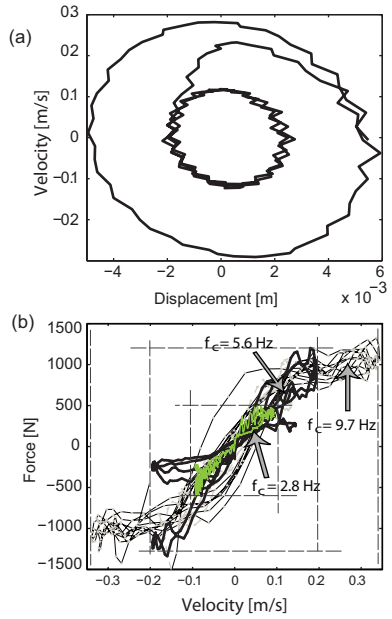

Fig. 5. Experiment # 21: (a) Computed velocity versus displacement ($f_c = 5.6$ Hz), (b) Force versus velocity plot for $f_c = 2.8$, $f_c = 5.6$ Hz, and $f_c = 9.7$ Hz. Dotted lines show the semi-active covering due to displacement amplitude variation.

The effect of the applied electric current and the frequency of the piston displacement on the hysteresis. Experiment # 22 shows that the electric current is inversely proportional to the hysteresis for frequencies below that of 7 Hz (Fig. 7a-7b), and proportional for frequencies above 7 Hz (see difference from Fig. 7b-7c). The electric current increases the yield point, which is the *MR* force value for a specific velocity when the transition from pre-yield to post-yield behavior happens. By contrast, the frequency of the piston displacement is proportional to the hysteresis, and the hysteresis increases with the frequency when no electric current is present, Fig. 7a.

Body temperature of the *MR* damper. A procedure is performed over the database in order to determine the effect of the *DoE* on the body temperature. The procedure is as follows: (a) obtain the increase rate of the body temperature for each experiment and their replicas; (b) perform a descendent sort on the *DoE* dataset by the increase rate of damper cylinder temperature and create a table; and (c) identify the displacement and electric current sequences that increase the body temperature. Fig. 8 shows the computed rates for each *DoE*. These rates allow to limit the time of experimentation when a specific *DoE* is used. This in order to keep the *MR* fluid in the span of *-40* to *150* ^oC. Other results are: (a) the displacement sequences *CHS, FM, AM*, and *SFS* in combination with the electric current sequences *ICPS* and *PRBS* present the highest temperature gradient; and (b) the *RP* displacements have the lowest temperature gradient for all the levels of the electric current.

Fig. 9 shows the temperature behavior of the *MR*

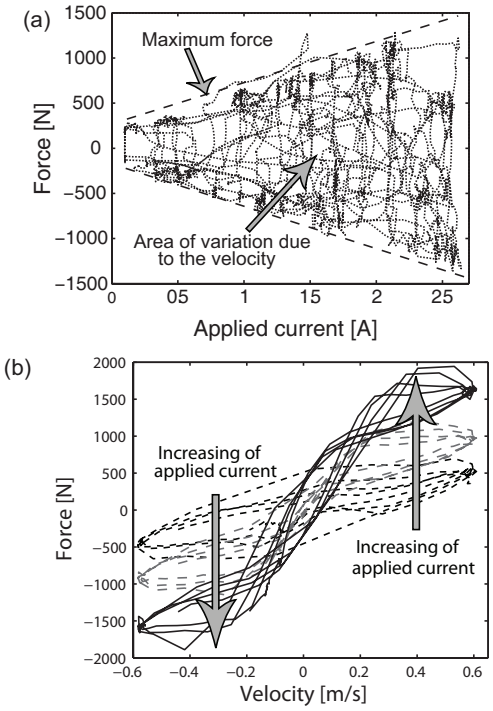

Fig. 6. Maximum f_{MR} versus electric current (a) and velocity (b).

damper body for Experiments # 10 and # 21 during all replicas. The rate of damper body temperature is also shown. Experiment # 21 shows that a carrier frequency over *6* Hz raises the rate of change of damper body temperature. On the other hand, for frequencies below *6* Hz, the rate is considerable lower. The results shows that the temperature is strongly dependent on the frequency of piston displacement , and in a minor way on the displacement amplitude. This is shown in Experiments # 17-19 that although they have a bandwidth of *0-15* Hz, their displacement magnitudes are small.

A second procedure studies the distribution of the measured damping force when the damper body is cold (first replica) and hot (last replica). This procedure uses the hypothesis Levene's test, (Brown and Forsythe, 1974), which is an inferential statistic used to assess the equality of variances in different samples. One advantage of Levene's test is that it does not require normality of the underlying data or when these data are prone to outliers. The hypothesis test is

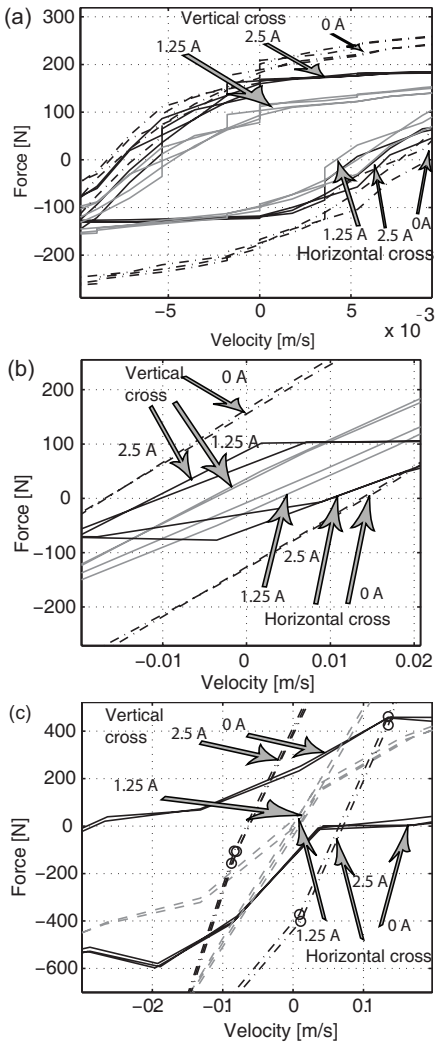

Fig. 7. Influence of the electric current and the frequency of the piston displacement on the hysteresis for Experiment # 22. The chosen frequencies are $f_c = \{1.5, 7, 14\}$ Hz corresponding to the a, b and c plots. The applied currents are $I = \{0, 1.2, 2.5\}$ A in each plot.

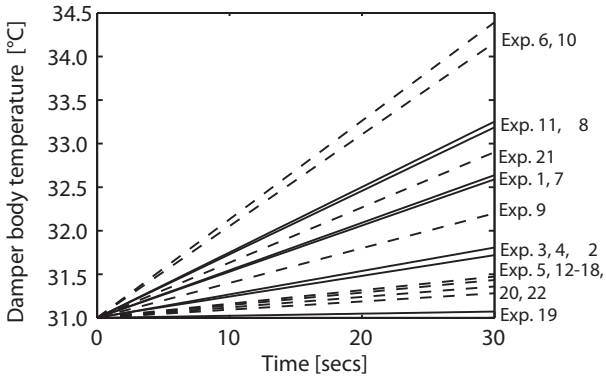

Fig. 8. Rates of damper body temperature. Right side indicates the corresponding *DoE*.

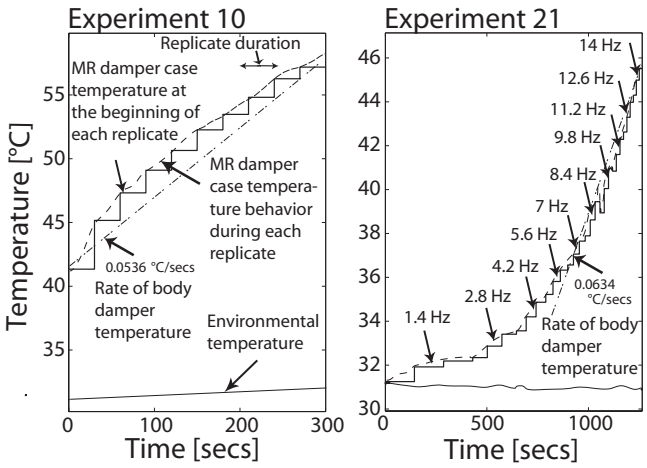

Fig. 9. Temperatures on the *MR* damper case and environmental.

done to the Experiments # 6 (it has the highest damper body temperature increase rate), # 3 (it has a middle damper body temperature increase rate), and # 12 (it has the lowest damper body temperature increase rate). In the three experiments, the null hypothesis is not rejected, hence although certainly the viscosity and temperature of the oil are well correlated, the temperature effect is negligible because the narrow range of operation. Given this result, any replica of the proposed *DoE*s can be used for *MR* damper modeling.

As a summary, the experimental database can expose the phenomena from the behavior of the *MR* damper in a wide manner and from several functional scenarios.

The experimentation of *MR* dampers aimed at obtaining models for simulation of driving conditions is not well addressed in literature. In fact, it is not a recurrent practice for typical damper. In vehicle dynamics simulation and evaluation, the basic damper as a linear device has only a damping coefficient. who is selected using an analysis of the whole vehicle. These damping coefficients can be: (a) low for comfort, (b) medium for straight driving on rough roads, and (c) high for best handling, (Dixon, 2007). When using a passive damper, there is a comfort/handling compromise which defines the baseline damper configuration. When using an *MR* damper, the vehicle suspension is called semiactive and the

mentioned compromise takes place in a control law in order to obtain the optimum damping according to the situation. In semiactive suspensions, the *MR* damper can be a *Continuously Controlled Damper (CCD)* (continuous variation of the manipulation), and an *On-Off Controlled Damper (On-Off CD)* (manipulation varies between two fixed values). Figure 10, shows a categorization of expected strokes and velocities in a piston damper for the specific driving conditions of a commercial vehicle, (Fukushima et al., 1983). This categorization can be extended to the *MR* damper using the stroke and velocity spans of the damper rod and their frequency content in order to propose subsets of experiments focused on the driving condition. According to the vehicle dynamics terminology *SAE J670* (Jan 2008), besides the driving conditions specified in Fig. 10, the target applications *body control*, *wheel hop* (best handling), and *wheel tramp* mitigation are of main interest when using semiactive suspensions. In addition, there is a lack of *MR* damper experimentation in order to obtain proper experimental data to be used in these target applications.

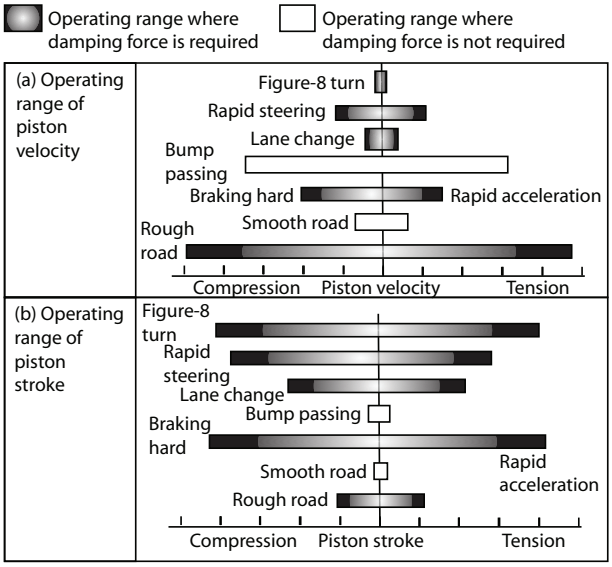

Fig. 10. Damping operating range for several driving conditions, (Dixon, 2007).

The body control refers to control of the bounce, pitch, and roll of a vehicle (called primary ride comfort). Wheel hop is the vertical oscillatory motion of a wheel between the road surface and the sprung mass. Wheel tramp is the form of wheel hop in which the wheels on an axle hop in opposite phase and it is present in solid axles. The resonant frequencies for most passenger cars range from 1-1.2 Hz for bounce motion, from 1.2-1.5 Hz for pitch motion, from 1.5-2 Hz for roll motion, and from 10-14 Hz for wheel hop (Barak, 1991). In the case of wheel tramp, a more typical rear suspension in pickups and rear-wheeled vehicles, the resonant frequency can be between 14-17 Hz, (Kramer et al., 1996). Using such categorization in Figure 10 and the optimum damper characteristics presented in (Fukushima et al., 1983) for a baseline damper, the characteristics of the tested *MR* damper are suggested. Based on Figure 11, an extension of the results (Fukushima et al., 1983) to a *MR* damper must be considered because the experimental velocities and strokes. Figure 11 shows the optimum *MR* damping characteristics for the categories shown in Figure 10 using a experimental dataset. As the short and long strokes require considerable differences in forces, the increase of electric current can achieve these differences. Once the resonance frequencies are known, as

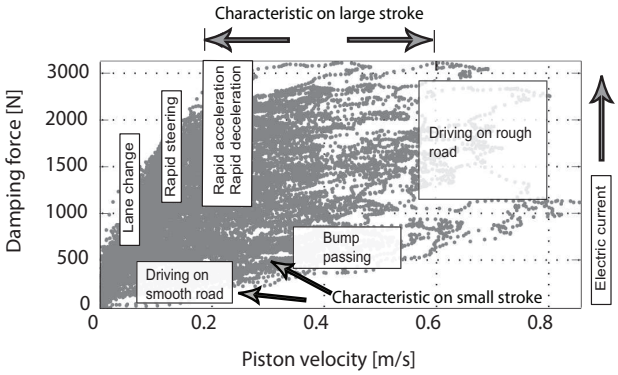

Fig. 11. Optimum *MR* damper characteristics, modified from (Dixon, 2007).

well as the stroke-velocity relations in several driving conditions, the next step is to know the domain of stroke, velocity, and frequency of the piston displacement for each experiment. The determination of the stroke and velocity domains requires the force-velocity and force-stroke (displacement) plots while the frequency content is obtained from the power spectral density computation. Table 6 shows the results of the categorization for driving conditions and target applications in vehicle dynamics analysis.

5 Case study

A set of experiments has been selected in order to perform identification and cross validation procedures. The *modified Semi-Phenomenological (SP)* and *maximum velocity MR* damper models, eqns (2-1) and (4-1) were identified using the least squares estimation. The identification procedure allows to obtain the model parameters for each selected experiment. The cross validation test consists on the evaluation of an identified model with a different experimental data. The Error-to-Signal Ratio (*ESR*) (5) (Savaresi et al., 2005), and the Relative Root-Mean-Square Error (*RRMSE*) (6) (Witters and Swevers, 2010) are two classical index performances.

$$SSE = \sum_{i}^{N} (\hat{f}_{MR_i} - f_{MR_i})^2, \; MSE = SSE/N$$
$$ESR = \frac{MSE}{\sigma_{f_{MR}}} \cdot 100\% \qquad (5)$$

Table 6. Categorization of experiments based on the target application. First column shows the application and driving conditions. Columns two and three define the recommend experiments for model identification to be utilized in close loop simulations of semiactive suspensions using *CCD* or *On-Off CD* manipulation. For open loop simulations, fourth column specifies the experiments using constant manipulations and fifth column shows the preferred electric current for each driving condition in order to assure comfort / handling. The numbers in second, third and fourth columns means the number of experiment. The *r-p* notation means from *r*-experiment and *p*-finishing.

Application	Close loop simulations		Open loop simulations	
Simulation / Modeling objective	*CCD*	On-Off *CD*	Constant damping	I [A]
Body Control *(BC)*	4,12, 21_2	5, 14	27-29	Variable
Wheel Hop *(WH)*	10,21_6-21_9	11	26	≥ 1.25
Wheel Tramp *(WT)*	10, 21_9, 21_{10}	11	26	≥ 1.25
Braking hard / Rapid acceleration *(BH / RA)*	4,5, 21_2	2	27-29	≥ 1.25
Figure-8 Turn *(F8T)*	8, 21_2	9	22, 27-29	≥ 1.25
Rapid Steering *(RS)*	8, 21_2	9	22, 27-29	≥ 1.25
Bump Passing *(BP)*	10, 21_4	11	26	0
Smooth Road *(SR)*	12, 19, 20, 21_2	14	18, 27-29	0
Rough Road *(RR)*	10, 21_6	11	26	≥ 1.25
Lane CHange *(LCH)*	12, 21_2	14	27-29	≥ 1.25
Normal driving conditions	12, 15, 16	14	27-29	Variable

$$RRMSE = \frac{\sqrt{SSE}}{\sqrt{\sum_i^N (f_{MR_i})^2}} \cdot 100\% \quad (6)$$

The cross validation intends to show the added-value of the *DoE* categorization for both models. For every model, the recommended *DoE* for a target applications with a continuous, on-off and constant damping are evaluated. Table 7 shows the results for *DoE*s with an electric current sequence in order to generate continuous and on-off controlled damping. Table 8 presents the results for *DoE*s with a constant electric current in order to generate a constant damping (soft or hard). *Target application* as row defines target application of the validation *DoE*. *Target application* as column defines the target application linked to the used *DoE* in the model identification. The column *DoE* specifies the used *DoE* in the model identification.

For instance, the *DoE*s 12 and 21_2 are recommended for the target applications *Body Control, Smooth Road, and Land Change (BC / SR / LCH)* when the expected electric current sequence generates a Controlled Continuous Damping. The validity of this recommendation is shown for the cross validation test of both models when they are identified with *DoE* 12 and 21_2 in Table 7, and they simulate the *MR* damping force generated several other experiments, including the *Classical DoE (CDoE)* 3. The recommended *DoE* has the lowest *ESR* while the others present higher *ESR*. These results are replicated when the index performance *RRMSE* is used, Table 9.

Another interesting result is the generalization of an *MR* damper model parameters when the identification is done with a specific *DoE*. Such *DoE* identifies parameters that allows high performances in f_{MR} estimation in a cross validation procedure. Fig. 12 shows the *ESR*s boxplot of both models. The validation *DoE* were those *DoE* used in tables 7 and 8. The *DoE*s in the horizontal axis were sorted in ascendent way according to the average *ESR* and only the firsts nine *DoE* are shown in the horizontal rank. The f_{MR} estimation with model parameters identified with the *DoE*s 4, 5, 21_4 shows a consistent low *ESR* average as well as the classic *DoE* 3 for the identified models. Several advantages of the new *DoE* proposals can be enumerated over the classical *DoE*: (a) the experimentation time is shorter in a 90% (*DoE*s 4, 5, 21_4), (b) the rate of temperature increase of the damper body are equal than classic *DoE* allowing a longer damper time life (*DoE* 4, 5), (c) they are easy implementable (*DoE*s 4, 5, 21_4).

Fig 13 shows a qualitative comparison when model parameters identified with Experiments # 3 and # 21 estimate the f_{MR} of Experiment #12. Subfigure (d) shows the piston velocity versus time. The subfigures array allows: to show the f_{MR} response when the electric current changes (subfigures (a) and (b)), the relation of transient piston velocity with the *F-V* plot (subfigures (c) and (d)), and finally, the estimation precision when the *modified SP* model is identified with the suggested experiment 21_2 and the estimation error when it is identified with the classical *DoE*, Experiment # 3, (subfigures (a) and (b)).

The maximum velocities for the damper rod, Fig. 13(d), allows to evaluate in a qualitative manner the *MR* damping estimation error in transient response, Fig. 13(a), and Force-Velocity characteristic, Figure 13(c). Later figures show that the model identification using Experiment # 21_2 allows a more accurate damper modeling. The model identification using Experiment # 3 computes a wrong *MR* damping force in peak velocities when the model estimates the damping

Table 7. Cross validation for the *modified SP* and *VMax MR* damper model parameters for continuous and On-Off damping. The results show the percentage of error for the *ESR* index performance. The rows define the *DoE* in the identification. The columns show the *DoE* for validation. A row with double line indicates when the *DoE* change the type of damping. The target applications are described by its acronyms according to Table 6.

Modified semi-phenomenological model											
Target application		**WT**	**WH / WT**			**WH / RR**	**BP**	**BC / SR / LCH**		**BH / RA**	**F8T / RS**	**CDoE**
Application	***DoE* with continuous controlled damping**											
	DoE	**21**$_{10}$	**10**	**21**$_7$	**21**$_9$	**21**$_6$	**21**$_4$	**12**	**21**$_2$	**4**		**3**
WT	**21**$_{10}$	2.7	26.6	10.7	4.1	13.6	32.1	132.7	97.9	91		89.4
WH / WT	**10**	9.8	6.4	4.6	7.1	3.5	3.7	16.1	9.9	9.9		10.6
WH / WT	**21**$_7$	7.2	7.8	4.0	5.2	3.6	6.8	32.4	22.6	21.1		21.8
WH / WT	**21**$_9$	3.3	17.1	6.7	3.4	8.1	19.6	86.9	61.9	59		58.6
BC / SR / LCH	**12**	60.3	45.5	24.1	41.9	17.2	6.6	6.8	5.1	25.5		27.1
BC / SR / LCH	**21**$_2$	178.2	157.3	73.9	123.7	51.5	19.4	10.6	6.9	83.1		96.1
BP	**21**$_4$	15.7	8.7	6.3	11.2	4.7	2.9	10.4	6.7	8.1		8.3
WH / RR	**21**$_6$	8.7	6.7	4.1	6.3	3.3	4.5	21.2	14.1	13.4		14.3
BH / RA	**4**	13.5	7.6	6.5	10.0	5.2	4.4	11.2	8.0	6.8		7.1
CDoE	**3**	15.8	8.3	7.9	11.9	6.4	5.5	12.0	9.4	7.3		6.7
Application	***DoE* with an on-off controlled damping**											
	DoE	**11**						**14**		**2**	**9**	**3**
BH / RA	**2**	10.6						17.1		8.6	13.5	7.3
F8T / RS	**9**	6.8						17.3		8.9	8.8	12.4
WH / WT / BP	**11**	6.8						17.4		12.9	9.0	12.3
BC / SR	**14**	28.8						7.7		13.1	40.4	13.8
CDoE	**3**	10.2						19.7		12.6	12.0	6.7

Maximum velocity model											
Target application		WT	**WH / WT**			**WH / RR**	**BP**	**BC / SR / LCH**		**BH / RA**	**F8T / RS**	**CDoE**
Application	***DoE* with continuous controlled damping**											
	DoE	**21**$_{10}$	**10**	**21**$_7$	**21**$_9$	**21**$_6$	**21**$_4$	**12**	**21**$_2$	**4**		**3**
WT	**21**$_{10}$	11.7	26.3	16.0	14.0	13.8	23.4	85.7	84.8	70.1		64.6
WH / WT	**10**	17.2	15.8	13.6	16.3	11.3	18.4	52.4	79.7	48.5		39.2
WH / WT	**21**$_7$	15.6	16.3	12.3	15.0	9.2	11.1	35.2	45.4	32.4		28.0
WH / WT	**21**$_9$	12.4	21.2	14.0	13.5	11.5	17.7	63.9	65.3	53.1		48.4
BC / SR / LCH	**12**	84.8	69.4	36.1	58.8	25.6	11.1	9.3	8.3	39.6		43.9
BC / SR / LCH	**21**$_2$	140.8	121.3	59.4	97.6	41.8	16.6	10.4	7.2	66.5		75.6
BP	**21**$_4$	27.7	21.5	15.1	21.7	11.0	7.3	13.9	17.1	18.2		17.3
WH / RR	**21**$_6$	16.4	16.3	12.4	15.4	9.1	9.8	30.1	38.7	28.3		24.6
BH / RA	**4**	24.2	20.7	16.8	20.9	13.9	10.8	14.3	12.2	13.5		14.9
CDoE	**3**	23.2	20.0	15.8	20.2	12.6	9.2	13.7	13.2	13.9		14.5
Application	***DoE* with an on-off controlled damping**											
	DoE	**11**						**14**		**2**	**9**	**3**
BH / RA	**2**	32.3						12.4		13.6	37.8	16.2
F8T / RS	**9**	18.7						25.1		22.3	12.7	19.0
WH / WT / BP	**11**	15.7						64.7		48.1	18.6	33.1
BC / SR	**14**	251.2						27.4		54.6	377.6	96.8
CDoE	**3**	23.7						12.5		15.1	22.1	14.5

Table 8. Cross validation for the *modified SP* and *VMax MR* damper model parameters for constant damping. The results show the percentage of error for the *ESR* index performance. The rows define the used *DoE* in the identification. The columns show the used *DoE* for validation. A row with double line indicates when the *DoE*s change the type of damping. The target applications are described by its acronyms according to Table 6.

Modified semi-phenomenological model				
Target application		**BP**	**BC / SR, LCH**	**CDoE**
Application	***DoE*s with soft damping**			
	DoE	$\mathbf{26}_1$	$\mathbf{27}_1$	**3**
BP	$\mathbf{26}_1$	12.6	44.5	52.7
SR	$\mathbf{27}_1$	93.7	23.5	41.0
CDoE	**3**	27.3	75.4	6.7
Target application		**WH / WT RR**	**BH / RA F8T / RS**	**CDoE**
Application	***DoE*s with hard damping**			
	DoE	$\mathbf{26}_5$	$\mathbf{27}_4$	**3**
WH / WT / RR	$\mathbf{26}_5$	0.7	3.2	8.6
F8T / LCH / RS	$\mathbf{27}_4$	3.7	1.5	9.0
CDoE	**3**	1.5	2.9	6.7
Maximum velocity model				
Target application		**BP**	**BC / SR, LCH**	**CDoE**
Application	***DoE*s with soft damping**			
	DoE	$\mathbf{26}_1$	$\mathbf{27}_1$	**3**
BP	$\mathbf{26}_1$	12.6	44.5	64.1
SR	$\mathbf{27}_1$	94.4	23.5	44.2
CDoE	**3**	48.4	33.7	14.5
Target application		**WH / WT RR**	**BH / RA F8T / RS**	**CDoE**
Application	***DoE*s with hard damping**			
	DoE	$\mathbf{26}_5$	$\mathbf{27}_4$	**3**
WH / WT / RR	$\mathbf{26}_5$	11.6	16.7	30.5
F8T / LCH / RS	$\mathbf{27}_4$	95.0	4.5	75.3
CDoE	**3**	11.8	7.5	14.5

from Experiment # 12. Emphasis is made in the Experiment # 3 has different and constant electric currents, and Experiment # 21_2 uses an *ICPS* sequence as electric current, Fig. 13(b). This suggests a necessity of a persistent electric current in *MR* damper experimentation for a better f_{MR} estimation, Fig. 13(c). This qualitative evaluation suggests the categorization of *DoE* can be a valid tool in vehicle model evaluation.

6 Conclusions

An experimental database with several experiments for *MR* dampers has been presented. An experiment categoriza-

Table 9. Cross validation for the *modified SP* and *VMax MR* damper model parameters for constant damping using the *RRMSE* as index performance. The rows define the used *DoE* in the identification. The columns show the used *DoE* for validation. The target applications are described by its acronyms according to Table 6.

Modified SP model						
Target application		**BH RA**	**BC / SR LCH**	**WH / WT RR**	**BH RA**	**CDoE**
	DoE	**4**	$\mathbf{21}_2$	$\mathbf{26}_5$	**2**	**3**
BH / RA	**4**	26.1	28.3	11.1	29.8	26.7
BC / SR LCH	$\mathbf{21}_2$	51.7	22.3	57.1	44.6	53.0
WH / WT RR	$\mathbf{26}_5$	28.8	26.3	8.3	32.9	29.2
BH / RA	**2**	27.0	29.7	13.8	29.3	26.9
CDoE	**3**	27.0	30.6	12.1	30.0	25.8
VMax model						
Target application		**BH RA**	**BC / SR LCH**	**WH / WT RR**	**BH RA**	**CDoE**
	DoE	**4**	$\mathbf{21}_2$	$\mathbf{26}_5$	**2**	**3**
BH / RA	**4**	36.7	34.8	34.3	37.7	38.5
BC / SR LCH	$\mathbf{21}_2$	91.8	27.8	111.7	73.8	98.2
WH / WT RR	$\mathbf{26}_5$	61.6	79.1	34.1	68.4	55.1
BH / RA	**2**	37.8	34.0	35.0	36.8	40.1
CDoE	**3**	37.3	36.2	34.3	38.9	38.0

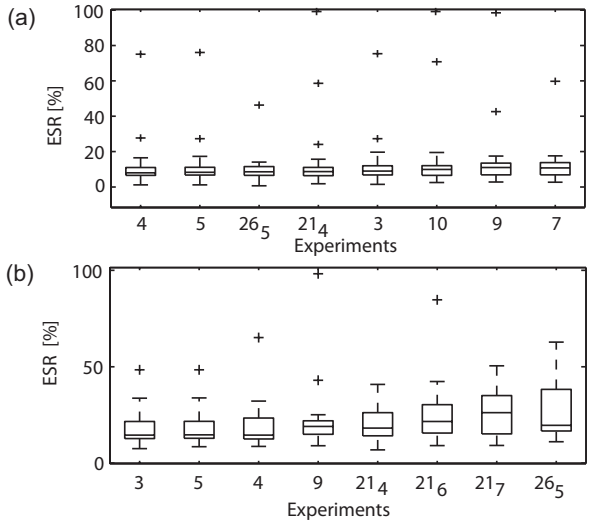

Fig. 12. Statistical performance of the *ESR* for cross validation of model parameters when they are identified with the new *DoE* and classical Experiment # 3. (a) shows the results for *modified SP* model and (b) shows *VMax* model. The horizontal axis shows the *DoE*. The vertical axis shows the *ESR* when the model estimates the f_{MR}.

tion was presented based on specific automotive applications. In order to show the potential of the generated experimental database, three experiments are analyzed showing the effects of the variation of the displacement amplitude and electric current when the frequency of piston displacement is constant, the exploration of all the modes of operation of the damper when the electric current and the amplitude displacement remain constant, and the excitation of the hysteresis due to a random frequency under sinusoidal displacement and a several levels of electric current. These specific experiments show the information of the *MR* damper force (f_{MR}) with the objective of a better understanding of the dynamic of this device and modeling it.

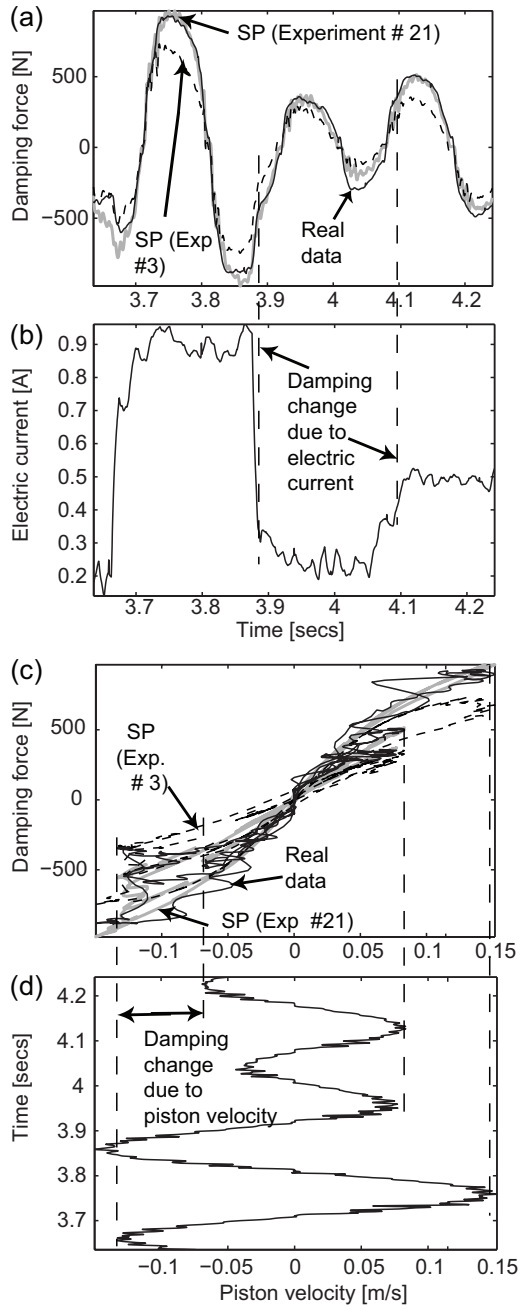

Fig. 13. The f_{MR} estimation using the modified SP model versus data from Experiment # 12 (smooth road). The modified SP model estimates the f_{MR} using two sets of parameters from Experiments # 21_2 and # 12. Subfigure (a) shows the f_{MR} transient response, subfigure (b) shows the applied electric current in the MR damper versus time, subfigure (c) presents the F-V plot of the estimated forces versus the measured one, and subfigure (c) shows the piston velocity versus time describing by dotted lines its relation with the maximum damping force.

The identification of two *MR* damper models using nineteen experiments validates the results. A cross validation test shows the categorization of the experiments as a tool for modeling. Also, it shows one of the proposed *DoE* gives better cross validation results in both validated models. The main contributions of this research are:

1. A Design of Experiments (*DoE*) for an *MR* damper modeling considering the target application of the model. The domain of these applications considers the control of semi-active suspensions where comfort and handling are goals under several drive conditions.
2. New guidelines of *DoE* for MR damper modelling that consider displacement and electric current sequences are validated.
3. The methodology can be tailored to another application or type of damper.

6.1 Further work

This study does not accomplish the correlation of the phenomenological relations and parameters design of dampers with the experimental results. This correlation is the subject of a further study. Tests in an industrial laboratory are mandatory.

Achnowledgements

Authors thank the PCP 2007-2011 (Programa de Cooperación del Posgrado, CONACYT) that partially supports the Tecnológico de Monterrey (Mexican side) and the Institut National Polytechnique de Grenoble (French side) during this research as an international collaborative project.

References

P. Barak. Magic Numbers in Design of Suspension for Passenger Cars. *SAE Society of Automotive Engineers Transactions (1991)*, 100(6):1698–1733, 1991.

Donald Bastow, Geoffrey Howard, and John P. Whitehead. *Car Suspension and Handling*. Pentech Press, London, 4^{th} edition, 2004.

M. J. L. Boada, Jose Antonio Calvo, Beatriz L. Boada, and Vicente Diaz. A New Non-Parametric Model Based on Neural Network for a MR Damper. In *ASME 2008* 9^{th} *Biennial Conf on Eng Sys Design and Analysis July 79, Israel*, 2008.

M. B. Brown and A. B. Forsythe. Robust Tests for the Equality of Variances. *J of the American Statistical Association*, 69(346): 364–367, 1974.

SA Burton, N Makris, I Konstantopoulos, and PJ Antsaklis. Modeling the Response of ER Damper: Phenomenology and Emulation. *Eng. Mech.*, 122:897–906, 1996.

C. Chang and Li Zhou. Neural Network Emulation of Inverse Dynamics for a MR Damper. *Struct. Eng.*, 128:231–239, 2002.

Sang-Won Cho, Byoung-Wan Kim, Hyung-Jo Jung, and In-Won Lee. Implementation of Modal Seismically Excited Structures using Magnetorheological Dampers. *J of Eng Mech ASCE*, 131(2):177–184, 2005.

S. B. Choi, Y. T. Choi, E. G. Chang, S. J. Han, and C. S. Kim. Control Characteristics of a Continuously Variable ER Damper. *Mechatronics*, 8(2):143–161, 1998.

S. B. Choi, S. K. Lee, and Y. P. Park. A Hysteresis Model for Field-Dependent Damping Force of a Magnetorheological Damper. *Sound and Vibration*, 245:375–383, 2001.

Seung-Bok Choi and Kum-Gil Sung. Vibration Control of Magnetorheological Damper System subjected to Parameter Variations. *Int. J. Vehicle Design*, 46(1):94–110, 2008.

J. G. S. da Silva. Dynamical Performance of Highway Bridge Decks with Irregular Pavement Surface. *Computers and Structures*, 82:871–881, 2004.

J. C. Dixon. *The Shock Absorber Handbook*. John Wiley and Sons Ltd, Professional Engineering Publishing, Windsor, UK, 2^{nd} edition, 2007.

Haiping Du, Kam Yim Szeb, and James Lam. Semi-Active H_1 Control of Vehicle Suspension with Magneto-Rheological Dampers. *J. of Sound and Vibration*, 283:981–996, 2005.

N. Fukushima, K. Hidaka, and K Iwata. Optimum Characteristics of Automotive Shock Absorbers under Various Driving Conditions and Road Surfaces. *International Journal of Vehicle Design*, 4(5):463–472, Sept 1983.

Shuqi Guo, Shapou Yang, and Cunzhi Pan. Dynamical Modeling of Magneto-rheological Damper Behaviors. *Int. Mater, Sys. and Struct.*, 17:3–14, 2006.

Hugh Herr and Ari Wilkenfeld. User-Adaptive Control of a Magnetorheological Prosthetic Knee. *Ind Robot: An Int J*, 30(1): 42–55, 2003.

Faycal Ikhouane, Victor Ma nosa, and José Rodellar. Adaptive Control of a Hysteretic Structural System. *Automatica*, 41: 225–231, 2005.

M. R. Jolly, J. W. Bender, and J. D. Carlson. Properties and Applications of Commercial Magnetorheological Fluids. In *SPIE 5^{th} Annual Int. Symposium on Smart Structures and Materials*, San Diego; CA, March 1998.

J-H Koo, F. D. Goncalves, and M. Ahmadian. A Comprehensive Analysis of the Response Time of MR Dampers. *Smart Mater. Struct.*, 15:351–358, 2006.

W.I. Kordonsky. Magnetorheological Effect as a Base of New Devices and Technologies. *J of Magnetism and Magnetic Materials*, 122(1–3):395–398, 1993.

D. Kowalski, M. D. Rao, J. Blough, and S. Gruenberg. The Effects of Different Input Excitations on the Dynamic Characterization of an Automotive Shock Absorber. SAE Technical Paper 2001-01-1442, 2001. DOI:10.4271/2001-01-1442.

K. D. Kramer, W. A. Janitor, and L. R. Bradley. Optimized Damping to Control Rear End Breakaway in Light Trucks. In *Int Truck and Bus Meeting and Exposition, Detroit, MI, Light Truck Suspensions (SP-1198), October 14-16*, 1996.

Alan Hiu-Fung Lam and Wei-Hsin Liao. Semi-Active Control of Automotive Suspension Systems with Magneto-Rheological Dampers. *Int J of Vehicle Design*, 33:50–73, 2003.

W. H. Li, G. Z. Yao, and G. Chen. Testing and Steady State Modeling of a Linear MR Damper under Sinusoidal Loading. *Smart Materials Structures*, 9:95–102, 2000.

J. de-J Lozoya-Santos, R Morales-Menendez, R A. Ramirez, and E Nino. Frequency and Current Effects in a *MR* Damper. *Int J of Vehicle Autonomous Systems*, 7(3/4):121–140, 2009a.

J. de-J. Lozoya-Santos, R. Morales-Menendez, and R. Ramirez-Mendoza. Magneto-Rheological Damper Modelling. In *International conference on modelling, simulation and validation, WorldComp09*, pages 92–98, Texas, USA, July 2009b.

J. de-J Lozoya-Santos, R. Morales-Menendez, and R. Ramirez-Mendoza. Design of Experiments for MR Damper Modelling. In *Neural Netwotks, 17^{th} IEEE Int. Joint Conf. on*, pages 1915–1922, Atlanta, USA, June 2009c.

J. de-J. Lozoya-Santos, R. Morales-Menendez, and R. A. Ramirez-Mendoza. MR-Damper based Control System. In *IEEE Int Conf On Systems, Man & Cybernetics*, pages 5168–5173, Texas, USA, October 2009d.

J. de-J. Lozoya-Santos, O. Sename, L. Dugard, R. Morales-Menendez, and R. Ramirez. A LPV Quarter of Car with Semiactive Suspension Model including Dynamic Input Saturation. In 4^{th} *IFAC Symp on System, Structure and Control*, Ancona, Italia, Sept. 2010.

N. Luo, J. Rodellar, J. Vehi, and M. de la Sen. Composite Semiactive Control of a Class of Seismically Excited Structures. *J of the Franklin Institute*, 338:225–240, 2001.

E. Nino, R. Ramirez, and D.Guerra. Application of Black Box Models for MR Damper Identification. In 1^{st} *MX Mechatronics, USA*, Philadelphia, USA, June 2006.

E Nino, R Morales-Menendez, R Ramirez, and L Dugard. Minimizing the Frequency in a Black Box Model of a MR Damper. In 11^{th} *Mini Conf on Vehicle Sys. Dyn., Ident. and Anomalies*, Budapest, Hungary, November 2008.

C. Poussot-Vassal, O. Sename, L. Dugard, P. Gáspár, Z. Szabó, and J. Bokor. A New Semi-Active Suspension Control Strategy through LPV Technique. *Control Eng Practice*, 16(12):1519–1534, 2008.

S. M. Savaresi, S. Bittanti, and M. Montiglio. Identification of Semi-Physical and Black-Box Non-Linear Models: the Case of MR-Dampers for Vehicles Control. *Automatica,*, 41(1): 113–127, 1 2005.

Sergio M. Savaresi and Cristiano Spelta. Mixed Sky-Hook and ADD: Approaching the Filtering Limits of a Semi-Active Suspension. *J. Dyn. Sys., Meas., Control*, 129(4):382–392, 2007.

A. C. Shivaram and K. V. Gangadharan. Statistical Modeling of a MR Fluid Damper using the Design of Experiments Approach. *Smart Mater. and Struct.*, 16(4):1310–1314, 2007.

Torsten Söderström and Petre Stoica. *System Identification*. Prentice Hall, Upper Saddle River, N. J., 1989.

X. Song and M. Ahmadian. An Adaptive Semiactive Control Algorithm for Magnetorheological Suspension Systems. *J of Vibration and Acoustics ASME*, 127(5):493–502, October 2005.

C. Spelta, F. Previdi, Sergio M. Savaresi, Guiseppe Fraternale, and Nicola Gaudiano. Control of Magnetorheological Dampers for Vibration Reduction in a Washing Machine. *Mechatronics*, 19: 410–421, 2009.

BF Spencer Jr, SJ Dyke, MK Sain, and JD Carlson. Phenomenological Model of a MR Damper. *J. Eng. Mech.*, 123(3):230–238, 1997.

R. Stanway, J. L. Sproston, and N. G. Stevens. Non-Linear Modelling of an Electro-Rheological Vibration Damper. *J of Electrostatics*, 20(2):167–184, December 1987.

D H Wang and W H Liao. Modeling and Control of Magnetorheological Fluid Dampers using Neural Networks. *Smart Mater. Struct.*, 14:111–126, 2005.

Dai-Hua Wang and Wei-Hsin Liao. Neural Network Modeling and Controllers for Magneto-Rheological Fluid Dampers. In *Fuzzy Systems, The 10^{th} IEEE International Conference on*, volume 3, pages 1323–1326, Melbourne, Australia, Dec. 2001.

J Wang, A Sano, T Chen, and B Huang. Blind Hammerstein Identificacion for MR Damper Modeling. In *American Control Conference (ACC 2007)*, pages 2277–2282, New York, USA, July 2007.

L. X. Wang and H. Kamath. Modelling Hysteretic Behavior in MR Fluids and Dampers using Phase-Transition Theory. *Smart Mater. Struct.*, 15:1725–1733, 2006.

Wang Wei and Xia Pinqi. Adaptive Control of Helicopter Ground Resonance with Magnetorheological Damper. *Chinese J of Aeronautics*, 20:501–510, 2007.

M. Witters and J. Swevers. Black-box Model Identification for a Continuously Variable Electro-Hydraulic Semi-Active Damper. *Mech Syst and Signal Proc*, 24(1):4–18, 2010.

J. Y. Wong. *Theory of Ground Vehicles*. John Wiley and Sons Inc, New York, USA, 2001.

Pin-Qi Xia. An Inverse Model of MR Damper using Optimal Neural Network and System Identification. *Sound and Vibration*, 266 (5):1009–1023, 10/2 2003.

Zhao-Dong Xu, Ya-Peng Shen, and Ying-Qing Guo. Semi-Active Control of Structures incorporated with Magnetorheological Dampers using Neural Networks. *Smart Mater. Struct.*, 12: 80–87, 2003.